28

Inter-Code Validation between NAL and DLR in the Aeroelastic Simulation for SST Configuration

Hamid Reza KHEIRANDISH[1], Wolfgang WEGNER[2], Ralph VOSS[2]
and
Jiro NAKAMICHI[3]

[1] Research Center of Computational Mechanics, Inc., Tokyo, Japan, hamid@rccm.co.jp
[2] German Aerospace Center(DLR), Goettingen, Germany, wolfgang@bambus.ae.go.dlr.de, ralph@fuchs.ae.go.dlr.de
[3] National Aerospace Laboratory, Tokyo, Japan, jiro@nal.go.jp

1.Introduction

One of the research topics still open to treat in the CFD area is to develop precise analytical code to calculate unsteady aerodynamics in transonic region due to control surfaces oscillation. The estimation of the aerodynamics of the control surfaces is a tough problem because the control surfaces are usually equipped along trailing edge and often are embedded in a developed boundary layer. This causes some difficulties to compute the unsteady aerodynamics due to the motion of the control surfaces. This research aims validation and/or improvement of the CFD codes through comparisons between either code-to-code and code-to-experimental data. This work has been done within a framework of Japan-Germany (NAL-DLR) cooperative research.

2.Outline of Test Model

Wind tunnel tests on an elastic half-span SST-type wing model were done for steady and unsteady cases with a fixed or forced oscillated control surface at NAL 2m x 2m transonic wind tunnel. The purpose of the tests was to accumulate the data base for verification of the CFD codes. The plan form and the dimensions of the model are shown in Fig.1.

The model is a semi-span arrow wing with a fuselage. The leading edge is double-swept-backed as shown in the figure. This wing has the NACA0003 airfoil section at each semi-span station. Unsteady flow fields are generated by harmonic oscillation of the aileron driven by an electric motor. The model is flexible, so that the dynamic deformations are induced due to the oscillation of the aileron.

The lowest natural frequency of the model is about 10 Hz in rest air. The total number of the pressure orifices is 46; 21 and 8 on the upper and the lower surfaces at 38% semi-span station and 9 and 8 at 75% semi-span station, respectively.

The dynamic deformation of the model as well as the unsteady aerodynamics was measured in the tests. The experimental results have already been published in Ref.[1]. For the present study, six tested cases, at Mach number 0.9 and 0.98 with the aileron frequencies from 5 to 25 Hz, have been selected as the validation data for the present studies.

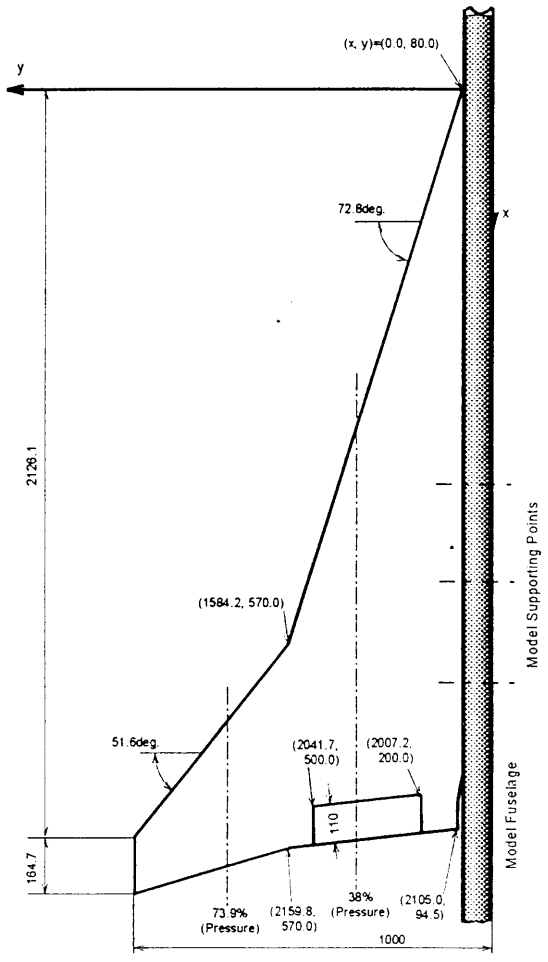

Fig.1 Outline of Tested Model

3.CFD Methods at NAL and DLR

The CFD methods of NAL and DLR are summarized in table 1. The NAL CFD code for flutter simulation is based on the 3D thin-layer approximated Navier-Stokes equations with the Baldwin-Lomax turbulence model[2] for the flow field and a modal approach formulation for the structural dynamics. The integration is performed employing the second-order accurate upwind TVD scheme[3] for the flow equations and the Wilson's θ method[4] for the equations of motions of the structure, respectively. The integration of the flow equations is proceeded on dynamic grids, in a time accurate manner. At NAL, the grids are regenerated at each time step fitting the instantaneous position of the aileron. More details will be found in Ref[5].

The CFD code employed by DLR is based on the 3D Euler equations with integral boundary layer coupling. The Euler solver uses an upwinding scheme based on Wegner's Riemann solver[6]. The time integration is performed on dynamic grids applying the virtual grid deformation technique. The boundary layer equations are solved in stream-line direction at every time step. The obtained boundary layer thickness is considered to correct the solid-wall boundary condition. In the virtual grid deformation technique the actual grid points are not needed. only the gradients of the metrics of the grid system and the grid speeds at each time step are used during the unsteady computations. These quantities are interpolated in space and can be obtained by sufficiently small additional computing time.

At NAL, an elastic wing simulation is also done by the use of the present code. In this case, the governing equations for flow field and the equations of motion of the structure are integrated simultaneously, coupling with each other. The dynamic deformation of the wing is supposed by superposing the fundamental vibration modes weighted by generalized coordinates.

4. Computed Cases

The computed cases are summarized in Table 2, along with the information on the flow conditions and the test parameters. The Reynolds number is fixed to 12 millions (based on the half root-chord-length) in all the computed cases, although its value will slightly differ from case by case in the experiments due to the changes of Mach numbers and dynamic pressures. Several steady and unsteady cases were numerically simulated by both NAL and DLR and the results are compared with each other as well as with the experimental results.

Table 1. Comparisons of CFD Methods Between NAL and DLR

	NAL	DLR
Flow Model	thin-layer approximated Navier-Stokes equations	Euler equations with boundary-layer correction
Turbulence Model	Baldwin-Lomax model	Drela-giles closing condition
Difference Method	Yee-Harten TVD Second order in space and time	upwinding Wegner's Rieman solver Second order in space and time
Integration	ADI Time Accurate	 Time accurate explicit dual time stepping
Grid	dynamic grid algebraic Interpolation 0.8 million points	virtual dynamic grid 0.3 million points
Structural Side	model analysis Wilson's θ method	
Computing Time	5 hours/case(NWT NAL)	40 minutes/case(NEC DLR)

Table 2. Studied Cases (α=0)

Case No.	Mach number M	Mean deflection angle of aileron (degree) δ	Amplitude of the Aileron Oscillation (degree)	Frequency (Hz) F	Rigid or Elastic	NAL or DLR	Exp. result available
s-1	0.9	0.0	—	—	R	NAL/DLR	O
s-2	0.9	5.0	—	—	R	NAL/DLR	O
s-3	0.98	0.0	—	—	R	NAL/DLR	—
u-1	0.9	0.0	2	5	R	NAL/DLR	O
u-2	0.9	0.0	2	15	R	NAL/DLR	O
u-3	0.9	0.0	2	25	R	NAL/DLR	O
u-4	0.9	5.0	2	25	R	NAL/DLR	O
u-5	0.98	0.0	2	15	R	NAL/DLR	—
u-6	0.9	0.0	2	15	E	NAL	O

5.Comparison of Results - Steady Cases -

In the first, the computed steady pressure distributions at Mach numbers 0.9 and 0.98 are shown in Figs.2-4 in comparisons with the experimental results. The angle of attack of the main surface is 0° in all the computed cases. The Fig.2-3 show the cases with the mean deflection angles of the aileron (DAoA) 0° and 5° , respectively. Fig.4 is provided to compare the two computed results by NAL and DLR, though the experimental data are not available. In the most of the tested cases, there existed no supersonic regions on the main and aileron surfaces and accordingly no shock waves were established. It is well known that the shock waves on the wing surface have a significant role in the transonic unsteady aerodynamics and that they cause the non-linearity. A H-H mesh topology with .8 millions grid was used in NAL computations. The DLR computations was performed on a C-H mesh with .3 millions grid.

In Fig.2, the computed results by NAL and DLR are in good agreements with each other. However, there are some discrepancies between the computational results and the

experimental ones near the hinge line of the control surface. The computed wing section geometry is not compatible with the actual model especially at the upstream gaps of the aileron which is not

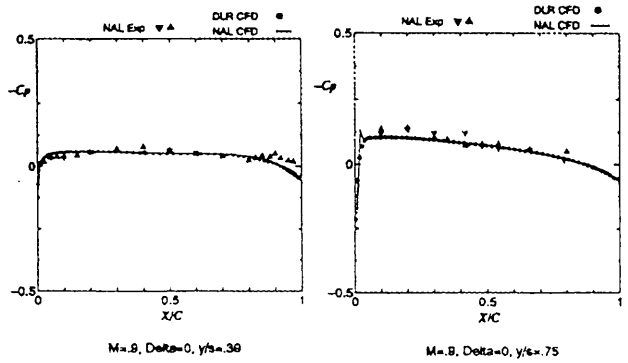

Fig.2 Comparisons Between CFD and Experimental Results (Steady Pressure Distributions)
(M=0.9, δ=0°, Re=1.2×10⁷)

simulated exactly in the numerical model. At 75% semi-span station, the agreement is much better because there is no longer the aileron there.

In Fig.3, the results for the DAoA, 5° are shown at Mach number 0.9. The measured pressure distributions do not coincide with the computed results concerning the pressure peak position, while the computed results by NAL and DLR show better agreement with each other. This is considered due to the same reason as the above. At 75% semi-span station, the experimental results are scattering, but they are relatively in good agreements with CFD results. In Fig.4, the computational results at Mach number 0.98 with DAoA, 0° are given. There are no significant differences between them.

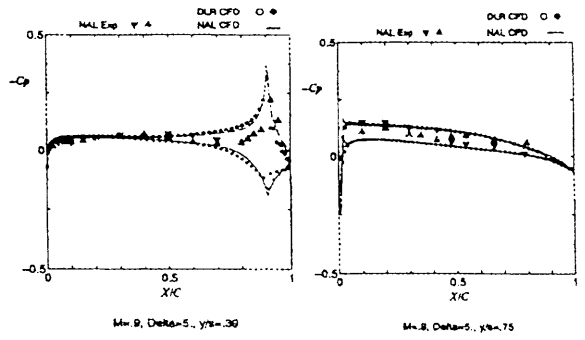

Fig.3 Comparisons Between CFD and Experimental Results. (Steady Pressure Distributions)
(M=0.9, δ=5°, Re=1.2×10⁷)

6. Comparison of Results - Unsteady Cases -

In these computations, the unsteady pressure distributions are decomposed into real and imaginary parts with respect to the aileron motion. The pressure data, for a cycle, are stored after when the solution get a steady periodic oscillation.

For the unsteady cases, the computed results on both upper and lower surfaces are indicated

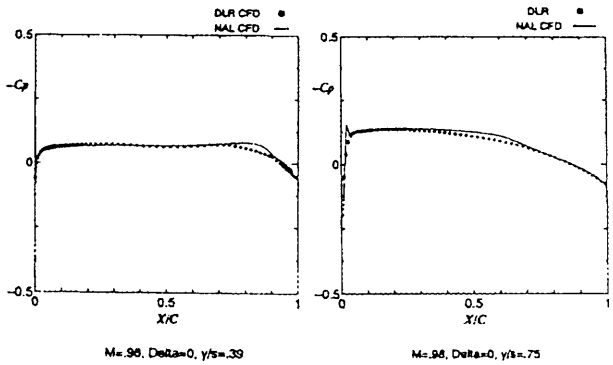

Fig.4 Comparisons Between CFD Results (Steady Pressure Distributions)
(M=0.98, δ=0°, Re=1.2×10⁷)

while the experimental data are given only for the upper surface. The amplitude of the aileron oscillation is 2° around the DAoA in all cases.

In Fig.5, the results of case No.U1 are shown. There are differences between the results obtained by NAL and DLR just upstream region of the hinge line. There are similar trends in the other cases going to be shown. The real parts computed by NAL are in a better agreement with the experimental ones.

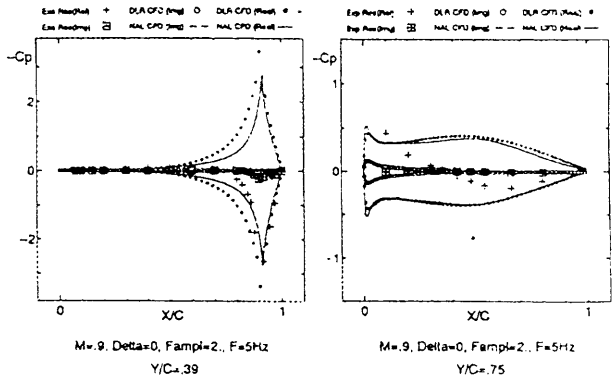

Fig.5 Comparisons Between CFD and Experimental Results -Unsteady Pressure Distributions-Real Part and Imaginary Part -
(M=0.9, A=2°, δ=0°, Re=1.2×10⁷, f=5Hz)

One of the reasons might be ; the governing equations in NAL code are Navier-Stokes equations while in DLR code they are Euler equations with the boundary layer correction; the other possible reason might be due to the difference in hinge line position of the aileron

between the NAL and DLR numerical models. The estimated boundary-layer thickness for the correction by DLR might be larger than that computed by NAL by solving the NS equations. At 75% semi-span station, the experimental results are far apart from the computed results. It comes from the fact that the pressure distributions were measured on the elastic wing while the wing is assumed rigid in the numerical simulations.

In Fig6, comparisons are shown for the case No. U2. The tendency is almost similar to the previous case. Here, too, especially the imaginary parts can not be compared well because of the effect of the elasticity of the wing. The wing is more violently excited in the case of the aileron frequency,15Hz, compared with the other cases. The lowest natural frequency comes up to about 13 Hz (close to excited frequency15Hz) in the flow with Mach number 0.9. So the dynamic deformation of the wing becomes considerably large in this case.

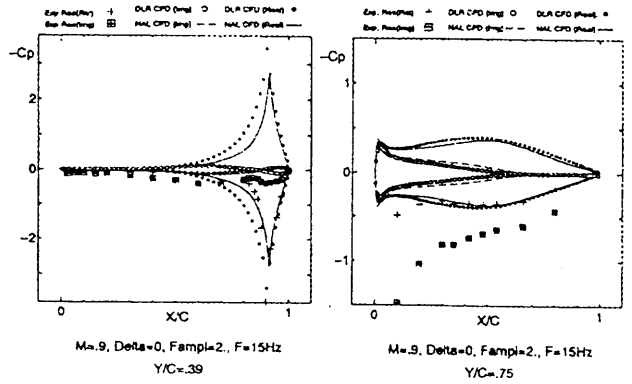

Fig.6 Comparisons Between CFD and Experimental Results-Unsteady Pressure Distributions-Real Part and Imaginary Part -
(M=0.9, A=2°, δ=0°, Re=1.2×10⁷, f=15Hz)

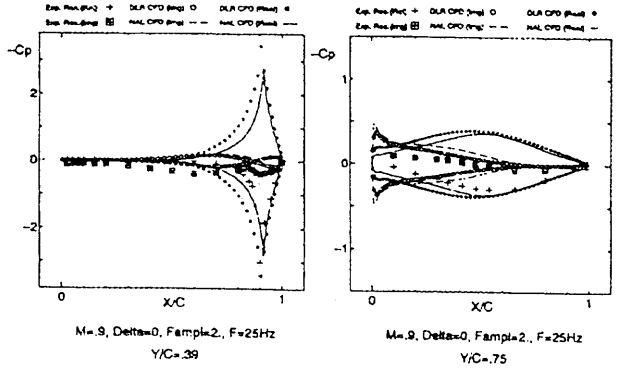

Fig.7 Comparisons Between CFD and Experimental Results-Unsteady Pressure Distributions-Real Part and Imaginary Part -
(M=0.9, A=2°, δ=0°, Re=1.2×10⁷, f=25Hz)

In Fig.7, Case No.U3 is shown. In this case, the imaginary parts are compared well because the amplitude of the wing response is small at the aileron frequency of 25Hz.

Fig.8 shows the case No.U4, in which the DAoA was taken to be 5°. In the cases of U1-U3, no significant supersonic regions were seen on the surface. It was expected in the case of U4 that a supersonic region appeared especially on the aileron surface. It can be confirmed from the steady pressure distributions(Fig.3) that the Cp is larger than the Cp critical,1.8 , on the aileron surface.

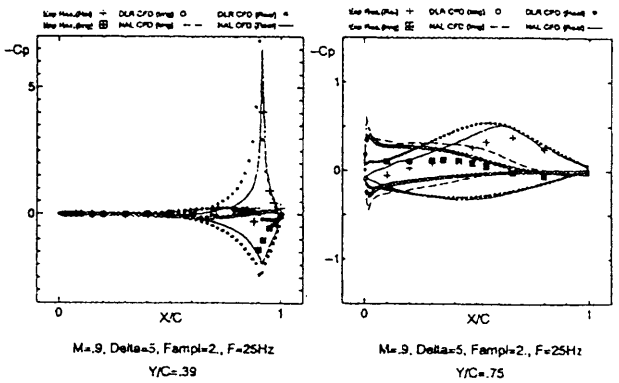

Fig.8 Comparisons Between CFD and Experimental Results-Unsteady Pressure Distributions-Real Part and Imaginary Part -
(M=0.9, A=2°, δ=5°, Re=1.2×10⁷, f=25Hz)

However, the unsteady pressure distributions do not explain the existence of the shock wave.

In figures 9.1-2, the steady Mach number contours are given to look at the flow patterns near and on the aileron surface. The free stream Mach numbers are 0.9 and 0.98 with the DAoA, 0° and 5°. In the cases of the DAoA, 5°, the contours are very dense especially near the hinge line and the aileron surface.

In Fig.10, the unsteady pressure distributions at Mach number, 0.98 are shown only for computed results. In this case, there are big differences between the results from NAL and DLR in the imaginary parts. The distributions of the unsteady components of the pressure distributions never show the existence of shock waves on the aileron surface, in this case too.

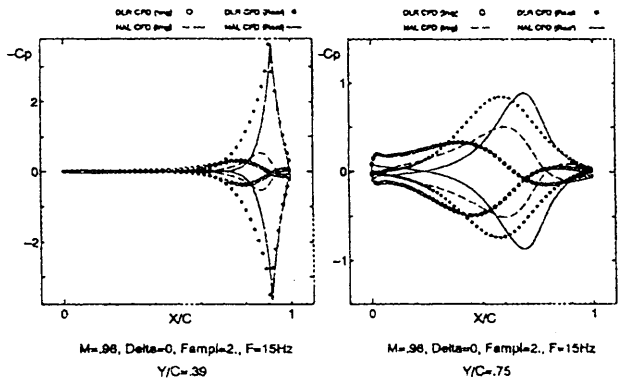

Fig.10 Comparisons Between CFD Results-Unsteady Pressure Distributions-Real Part and Imaginary Part - (M=0.98, A=2 ° , δ =0 ° , Re=1.2×10⁷ , f=15Hz)

One of the facts noted in the present studies is that there are no significant non-linearity in the unsteady pressure distributions regarding with the studied arrow wing.

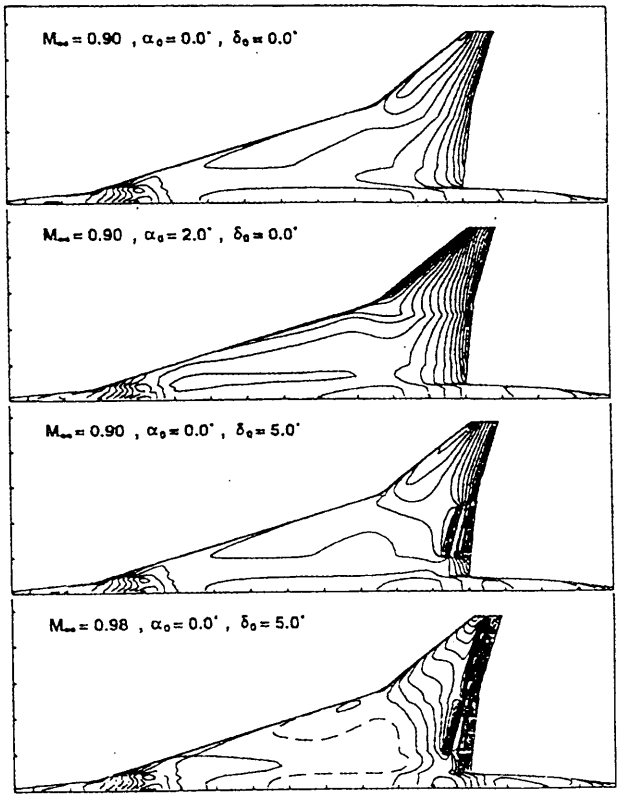

Fig9.1. Mach Contours (DLR CFD Results)

In Fig.11, higher order components of the unsteady pressure distributions determined by DLR are shown. It can be concluded from these figures that the effect of the non-linearity is very small even at high Mach numbers. The reason can be suggested as the thickness-to-chord ratio of the main surface for supersonic transport is too small (that is around 3%) to cause non-linear effect at the mentioned Mach number regions and conditions.

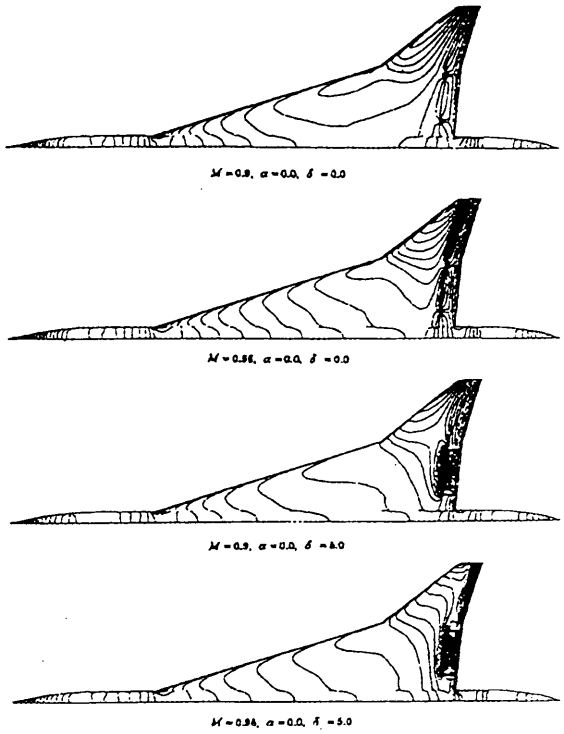

Fig9.2. Mach Contours (NAL CFD Results)

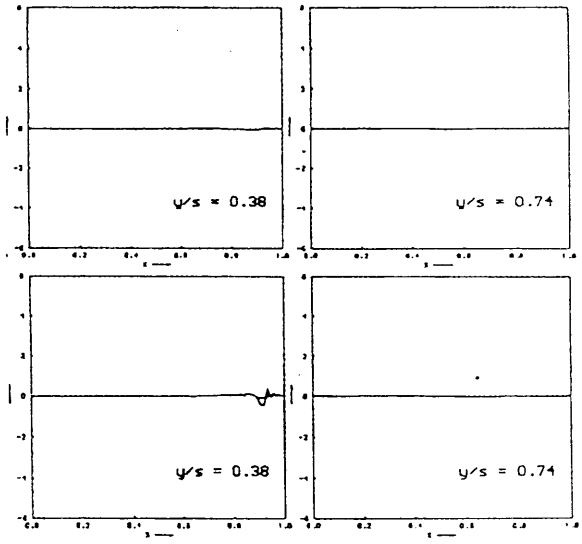

Fig 11. Second Harmonic of Unsteady pressure Upper)In Phase, Lower)Out of Phase (M=0.9, A=2 ° , δ =5 ° , Re=1.2×10⁷ , f=25Hz)

Finally, computational results in which the effect of the flexibility of the surface is taken into account are shown (case No. U6). These calculations were done by NAL. In the aeroelastic simulation, the first eight natural modes, which are obtained from FEM structural analysis, are superposed to approximate the aeroelastic response or the

static deformation of the wing.

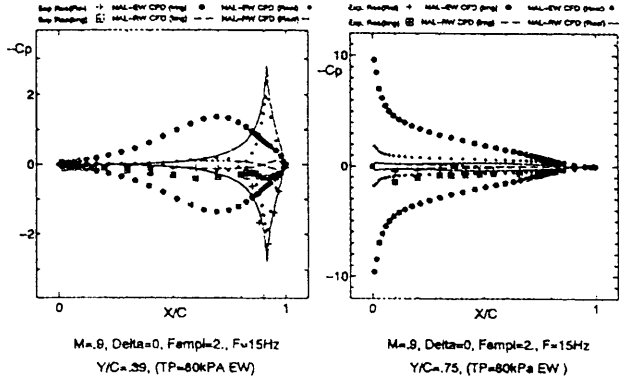

Fig.12 Comparisons Between CFD Results-Unsteady Pressure Distributions-Real Part and Imaginary Part - (M=0.9, A=2°, δ =0°, Re=1.2×10', f=15Hz, P_0=80kPa)

The computed results are shown in Fig. 12 with respect to real parts and the imaginary parts. These results are interestingly compared with the results shown in Fig.6 where the wing is treated as a rigid model. Especially the imaginary parts are improved in their distribution patterns although the comparisons with the experimental results are not sufficient.

In Fig. 13, the simulation results are lined up at in a series of time history of the pressure distributions at 39% semi-span station at every 1/8 phase, showing the phase of the aileron motion, in comparisons with measured data. The ΔCp describes the pressure coefficient subtracted by steady counterpart one. The number of the pressure orifices are so small that it is difficult completely to make the comparisons. In the figures, the dark areas show the instantaneous pressure distribution on the upper surface while the white ones are for the lower. The peak values at the hinge line are less estimated by the computations than the measured values. This simulation will be demonstrated by video film at the meeting.

Concluding Remarks

An unsteady experimental data base has been used for validating the CFD codes developed at NAL and DLR. Regarding the comparisons and discussions of results the followings are concluded

1. No significant differences between the results computed by NAL and DLR were observed.
2. The prediction of unsteady aerodynamics around control surfaces are still difficult.
3. The responses are almost linear even at high Mach number.

References

[1] Tamayama, M., Saitoh, K., Matsushita, H. and Nakamichi, J., "Data Set: SST Arrow Wing, Oscillating Flap," AGARD Unsteady Aerodynamics Working Group 22.

[2] Baldwin, B.S. and Lomax, H. "Thin Layer Approximation and Algebraic Model for Separated Turbulent Flows", AIAA Paper 78-257, 1978.

[3]Yee, H. and Harten, A, "Implicit TVD Schemes for Hyperbolic Conservation Law in Curvilinear Coordinates", AIAA Paper 85-1513.

[4] Bate, K.J. and Wilson, E.L. Mumerical Methods in Finite Element Analysis, Prentic-Hall, 1976.

[5] Kkeirandish, H., Goro, B. and Nakamichi, J., "Numerical Investigation of Flutter" ,International Journal of Computational Fluid Dynamics

[6] Wegner, W., "Aerodynamics for Elastically Oscillating Wings Using the Virtual Grid Deformation Method", report r-822, 85th AGARD/RTO Meeting, Aalborg, 1997

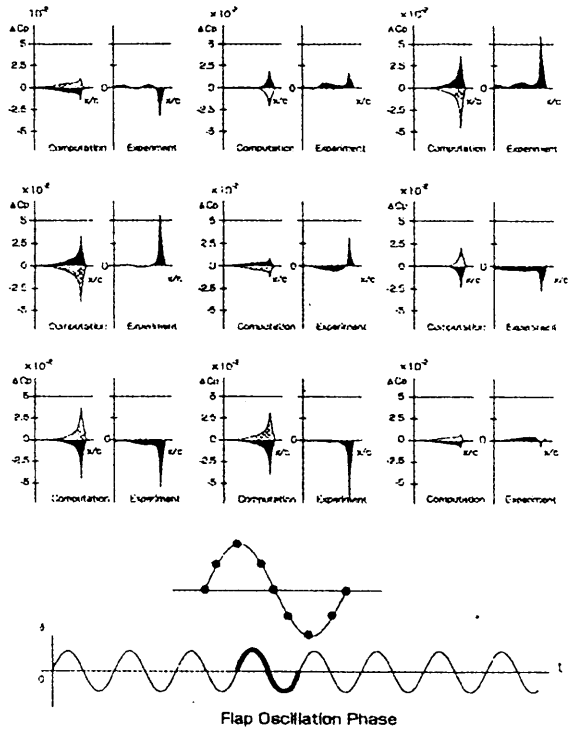

Fig. 13 Comparisons Between CFD and Experimental Results in Unsteady Pressure Distributions (M=0.9, A=2°, δ =0°, Re=1.2×10', f=15Hz, P_0=80kPa)